Volumetric HiLo microscopy employing an electrically tunable lens

Katrin Philipp,[1,*] Andre´ Smolarski,[1] Nektarios Koukourakis,[1] Andreas Fischer,[1] Moritz Stürmer,[2] Ulrike Wallrabe,[2] and Jürgen W Czarske[1]

[1]*Laboratory for Measuring and Sensor System Techniques, Technische Universitt Dresden, 01062 Dresden, Germany*
[2]*Laboratory for Microactuators, IMTEK, University of Freiburg, 79110 Freiburg, Germany*
[*]*katrin.philipp@tu-dresden.de*

Abstract: Electrically tunable lenses exhibit strong potential for fast motion-free axial scanning in a variety of microscopes. However, they also lead to a degradation of the achievable resolution because of aberrations and misalignment between illumination and detection optics that are induced by the scan itself. Additionally, the typically nonlinear relation between actuation voltage and axial displacement leads to over- or under-sampled frame acquisition in most microscopic techniques because of their static depth-of-field. To overcome these limitations, we present an Adaptive-Lens-High-and-Low-frequency (AL-HiLo) microscope that enables volumetric measurements employing an electrically tunable lens. By using speckle-patterned illumination, we ensure stability against aberrations of the electrically tunable lens. Its depth-of-field can be adjusted a-posteriori and hence enables to create flexible scans, which compensates for irregular axial measurement positions. The adaptive HiLo microscope provides an axial scanning range of 1 mm with an axial resolution of about 4 µm and sub-micron lateral resolution over the full scanning range. Proof of concept measurements at home-built specimens as well as zebrafish embryos with reporter gene-driven fluorescence in the thyroid gland are shown.

OCIS codes: (180.2520) Fluorescence microscopy; (180.6900) Three-dimensional microscopy; (220.1080) Active or adaptive optics; (100.6890) Three-dimensional image processing.

References and links

1. J. Mertz, *Introduction to Optical Microscopy* (Roberts, 2010).
2. M. Minsky, "Memoir on inventing the confocal scanning microscope," Scanning **10**, 128–138 (1988).
3. C. Cremer and T. Cremer, "Considerations on a laser-scanning-microscope with high resolution and depth of field," Microscopica Acta **81**, 31–44 (1974).
4. J. Huisken, J. Swoger, F. Del Bene, J. Wittbrodt, and E. H. K. Stelzer, "Optical sectioning deep inside live embryos by selective plane illumination microscopy," Science **305**, 1007–1009 (2004).
5. H.-U. Dodt, U. Leischner, A. Schierloh, N. Jährling, C. P. Mauch, K. Deininger, J. M. Deussing, M. Eder, W. Zieglgänsberger, and K. Becker, "Ultramicroscopy: three-dimensional visualization of neuronal networks in the whole mouse brain," Nature Methods **4**, 331–336 (2007).
6. M. A. A. Neil, R. Juskaitis, and T. Wilson, "Method of obtaining optical sectioning by using structured light in a conventional microscope," Opt. Lett. **22**, 1905 (1997).
7. P. J. Verveer, Hanley. Q. S., P. W. Verbeek, L. J. Van Vliet, and T. M. Jovin, "Theory of confocal fluorescence imaging in the programmable array microscope (PAM)," Journal of Microscopy **189**, 192–198 (1998).
8. C. Ventalon and J. Mertz, "Quasi-confocal fluorescence sectioning with dynamic speckle illumination," Opt. Lett. **30**, 3350 (2005).

#265224 Received 16 May 2016; accepted 20 Jun 2016; published 23 Jun 2016

9. D. Lim, K. K. Chu, and J. Mertz, "Wide-field fluorescence sectioning with hybrid speckle and uniform-illumination microscopy," Opt. Lett. **33**, 1819–1821 (2008).
10. J. W. Goodman, *Speckle Phenomena in Optics: Theory and Applications* (Roberts and Company Publishers, 2007).
11. J. W. Goodman, "Dependence of image speckle contrast on surface roughness," Opt. Commun. **14**, 324–327 (1975).
12. D. Lim, T. N. Ford, K. K. Chu, and J. Mertz, "Optically sectioned in vivo imaging with speckle illumination HiLo microscopy," J. Biomed. Opt. **16**, 016014 (2011).
13. J. Mertz and J. Kim, "Scanning light-sheet microscopy in the whole mouse brain with HiLo background rejection," J. Biomed. Opt. **15**, 16027 (2010).
14. T. N. Ford, D. Lim, and J. Mertz, "Fast optically sectioned fluorescence HiLo endomicroscopy," J. Biomed. Opt. **17**, 21105–21107 (2012).
15. M. A. Lauterbach, E. Ronzitti, J. R. Sternberg, C. Wyart, and V. Emiliani, "Fast Calcium Imaging with Optical Sectioning via HiLo Microscopy," PloS one **10**, e0143681 (2015).
16. N. Koukourakis, M. Finkeldey, M. Stürmer, C. Leithold, N. C. Gerhardt, M. R. Hofmann, U. Wallrabe, J. W. Czarske, and A. Fischer, "Axial scanning in confocal microscopy employing adaptive lenses (CAL)," Opt. Express **22**, 6025–6039 (2014).
17. M. Duocastella, G. Vicidomini, and A. Diaspro, "Simultaneous multiplane confocal microscopy using acoustic tunable lenses," Opt. Express **22**, 19293–19301 (2014).
18. S. A. Khan and N. A. Riza, "Demonstration of a no-moving-parts axial scanning confocal microscope using liquid crystal optics," Opt. Commun. **265**, 461–467 (2006).
19. Y. Nakai, M. Ozeki, T. Hiraiwa, R. Tanimoto, A. Funahashi, N. Hiroi, A. Taniguchi, S. Nonaka, V. Boilot, R. Shrestha, J. Clark, N. Tamura, V. M. Draviam, and H. Oku, "High-speed microscopy with an electrically tunable lens to image the dynamics of in vivo molecular complexes," Rev. Sci. Instrum. **86**, 013707 (2015).
20. T. Hinsdale, B. H. Malik, C. Olsovsky, J. A. Jo, and K. C. Maitland, "Volumetric structured illumination microscopy enabled by a tunable-focus lens," Opt. Lett. **40**, 4943–4946 (2015).
21. F. O. Fahrbach, F. F. Voigt, B. Schmid, F. Helmchen, and J. Huisken, "Rapid 3D light-sheet microscopy with a tunable lens," Opt. Express **21**, 21010–26 (2013).
22. J. Goodman, *Introduction to Fourier Optics* (McGraw-Hill, 1996).
23. J. Draheim, F. Schneider, T. Burger, R. Kamberger, and U. Wallrabe, in 2010 International Conference on Optical MEMS and Nanophotonics (OPT MEMS), (2010), pp. 15–16.
24. S. J. Kirkpatrick, D. D. Duncan, and E. M. Wells-Gray, "Detrimental effects of speckle-pixel size matching in laser speckle contrast imaging," Opt. Lett **33**, 2886–2888 (2008).
25. M. Imai, "Statistical properties of optical fiber speckles," Bulletin of the Faculty of Engineering, Hokkaido University **130**, 89–104 (1986).
26. P. A. Stokseth, "Properties of a Defocused Optical System*," Journal of the Optical Society of America **59**, 1314 (1969).
27. D. Kang, E. Clarkson, and T. D. Milster, "Effect of optical aberration on Gaussian laser speckle," Opt. Express **17**, 3084–3100 (2009).
28. B. Amos, G. McConnell, and T. Wilson*Comprehensive Biophysics* (Elsevier, 2012).
29. R. Opitz, E. Maquet, J. Huisken, F. Antonica, A. Trubiroha, G. Pottier, V. Janssens, and S. Costagliola, "Transgenic zebrafish illuminate the dynamics of thyroid morphogenesis and its relationship to cardiovascular development," Developmental biology **372**, 203–216 (2012).
30. N. C. Shaner, R. E. Campbell, P. A. Steinbach, B. N. G. Giepmans, A. E. Palmer, and R. Y. Tsien, "Improved monomeric red, orange and yellow fluorescent proteins derived from Discosoma sp. red fluorescent protein," Nature Biotech. **22**, 1567–1572 (2004).

1. Introduction

Wide field microscopy is well-established in biological and medical applications. At thick samples, however, wide field microscopy suffers from background signals and thus poor contrast and missing depth resolution [1]. In order to provide optical sectioning, many microscopic techniques have been introduced. The most prominent technique is confocal laser scanning microscopy [2, 3], often simply referred to as confocal microscopy. The principle of confocal microscopy is based on the illumination with a diffraction-limited spot and a pinhole-based detection, efficiently eliminating out-of-focus contributions from the sample. Confocal microscopy enables the acquisition of high-contrast, high-resolution data. However, the measurement rates of confocal microscopy are limited, because scanning is required to perform three-dimensional measurements.

#265224 Received 16 May 2016; accepted 20 Jun 2016; published 23 Jun 2016

In order to achieve higher measurement rates, alternative techniques rely on illuminating a bigger part of the sample and employing a camera for parallel light detection. For instance, light sheet microscopy is based on only illuminating a thin sheet of the sample and a camera detection [4, 5]. However, light sheet microscopy requires a second optical access and absorption of the light sheet becomes a problem for samples with large lateral dimensions. Another camera-based approach is the patterned illumination at the focal plane, which is used in structured illumination microscopy (SIM) [6] and programmable array microscopy (PAM) [7]. However, these techniques depend heavily on the delivery of a well-defined patterned illumination into the sample. Scattering and aberrations induced by the sample soften the contrast of the patterned illumination and lead to a decreased optical sectioning quality.

Techniques based on speckle illumination like dynamic speckle illumination [8] and High-and-Low-frequency (HiLo) microscopy [9] do not require well-defined nor controlled illumination, because the statistical properties of fully-developed speckles are unaffected by scattering and aberrations [10, 11]. However, the dynamic speckle illumination microscopy requires several images in order to reconstruct the high-frequency component of the images. This leads to a slow data acquisition, if the images are obtained over time or loss in spatial resolution, if the evaluation is conducted in space. The HiLo imaging technique relies on the acquisition of a second image with uniform illumination to obtain the high-frequency information of the image. The HiLo technique with speckled illumination was first proposed by Lim et. al [9] and successfully implemented in fluorescence microscopy [12], light sheet microscopy [13] and endomicroscopy [14]. Here, the sample is illuminated by a speckle patterned illumination generated by a laser. The contrast of the speckle illumination is high for the in-focus regions and low for the out-of-focus regions of the sample. As a consequence, the speckle contrast serves as a weighting function for filtering the out-of-focus contributions of the sample.

While HiLo microscopy provides optically sectioned images with wide field-of-view and high speed [15], axial scanning is required for volumetric imaging. Conventionally, this is done by mechanically moving either the objective or the sample. However, some samples are too sensitive to be moved. Moving the objective is slow for heavy objectives due to inertia and might lead to motion artifacts. Recently, a variety of microscopes such as confocal microscopy [16, 17, 18], wide field microscopy [19], structured illumination microscopy [20] and light sheet microscopy [21] benefited from using electrically or acoustically tunable lenses for axial scanning. However, as shown in [16] for confocal microscopy, the axial resolution degrades with increasing actuation voltages due to increasing aberrations of the tunable lens. In contrast, HiLo microscopy is expected to be robust against a degradation of the axial resolution due to aberrations, since the speckles that are used for the optical sectioning in the HiLo algorithm are invariant to aberrations and scattering in the sample (as long as the speckles are fully developed [10, 11]). Another challenge of using tunable lenses for axial scanning is the nonlinear relation between actuation voltage and axial displacement. This leads to irregular axial measurement positions and thus over- or under-sampled frame acquisition. Again, HiLo is capable of overcoming this limitation because its depth-of-view can be adjusted a-posteriori.

In this paper, we introduce an adaptive lens HiLo (AL-HiLo) microscope that enables volumetric measurements by employing an electrically tunable lens for axial scanning. We demonstrate that the AL-HiLo compensates for the nonlinear relation between actuation voltage and axial displacement as well as for the aberrations induced by the tunable lens. The performance of the setup is characterized and an analysis is given towards the realization of high-throughput scans in zebrafish embryos with reporter gene-driven fluorescence in the thyroid gland. In Section 2, the theoretical aspects of the HiLo technique are covered. The setup of the AL-HiLo microscope and characteristics of the electrically tunable lens are described in Section 3. In Section 4, the measurement system is characterized and exemplary measurements are presented

#265224 Received 16 May 2016; accepted 20 Jun 2016; published 23 Jun 2016

in Section 5. Finally, the results are discussed and an outlook is given in Section 6.

2. HiLo microscopy

HiLo microscopy is based on the acquisition of two images with different type of illumination in order to obtain one optically sectioned image. A uniform-illumination image is used to obtain the high-frequency (Hi) components of the image, and a nonuniform-illumination image is used to obtain the low-frequency (Lo) components of the image. The corresponding intensity distributions of the uniform- and nonuniform-illumination images are denoted as $I_{\mathrm{u}}(\vec{r})$ and $I_{\mathrm{n}}(\vec{r})$, respectively. The intensity distributions of the high- and low-frequency images are referred to as $I_{\mathrm{Lo}}(\vec{r})$ and $I_{\mathrm{Hi}}(\vec{r})$ with the spatial, two-dimensional coordinates $\vec{r}$. The resulting full-frequency optically sectioned image is then obtained by

$$I_{\mathrm{HiLo}}(\vec{r}) = I_{\mathrm{Hi}}(\vec{r}) + \eta I_{\mathrm{Lo}}(\vec{r}), \tag{1}$$

with η being a scaling factor that depends on the experimental configuration of the setup.

In order to obtain the high-frequency in-focus components, a typical characteristic of the optical transfer function (OTF) of a standard widefield microscope is exploited: high-frequency components are only well-resolved as long as they are in-focus while low-frequency components remain visible even if they are out-of-focus [22]. Hence, high-frequency components are directly extracted from $I_{\mathrm{u}}(\vec{r})$ using

$$I_{\mathrm{Hi}}(\vec{r}) = HP\{I_{\mathrm{u}}(\vec{r})\}, \tag{2}$$

whereby HP denotes a Gaussian high-pass filter with the cutoff frequency κ_c applied in the frequency domain.

The low-frequency component of the image is obtained by calculating

$$I_{\mathrm{Lo}}(\vec{r}) = LP\{C_{\mathrm{S}}(\vec{r}) I_{\mathrm{u}}(\vec{r})\} \tag{3}$$

with the complimentary low-pass filter LP. The speckle contrast $C_{\mathrm{S}}(\vec{r})$ acts as a weighting function for extracting the in-focus contributions and rejecting the out-of-focus contributions of the uniform-illumination image $I_{\mathrm{u}}(\vec{r})$. The overall spatial contrast $C_{\mathrm{n}}(\vec{r})$ is influenced by the speckles in the illumination as well as sample-induced speckles. In order to correct the influence of the sample-induced speckles, the difference image

$$I_{\delta}(\vec{r}) = I_{\mathrm{n}}(\vec{r}) - I_{\mathrm{u}}(\vec{r}) \tag{4}$$

is used for speckle contrast calculation. The speckle contrast is defined as

$$C_{\mathrm{S}}(\vec{r}) = \frac{\langle \sigma_{\delta}(\vec{r}) \rangle_A}{\langle I_{\mathrm{n}}(\vec{r}) \rangle_A}, \tag{5}$$

where $\langle I_n(\vec{r}) \rangle_A$ and $\langle \sigma_{\delta}(\vec{r}) \rangle_A$ are the mean of $I_n(\vec{r})$ and the standard deviation of $I_{\delta}(\vec{r})$, respectively. The speckle contrast is calculated over a partition of local evaluation areas A. It is assumed that each area is large enough to encompass several imaged speckle grains. The axial resolution is further increased by applying the band-pass filter

$$W(\vec{\kappa}) = \exp\left(-\frac{|\kappa^2|}{2\sigma_w^2}\right) - \exp\left(-\frac{|\kappa^2|}{\sigma_w^2}\right) \tag{6}$$

to the difference image $I_{\delta}(\vec{r})$ before evaluating $\langle \sigma_{\delta}(\vec{r}) \rangle_A$ [9]. As a result, the optical sectioning depth of the Lo-component can be adjusted by tuning σ_w. In order to also adjust the optical

#265224 Received 16 May 2016; accepted 20 Jun 2016; published 23 Jun 2016

sectioning depth of the Hi-component, the cutoff frequency of the Gaussian high pass filter is also tuned by setting $\kappa_c = 0.18\sigma_w$ [9].

Since the high- and low-frequency components of the image are now determined, the resulting optically sectioned HiLo image I_{HiLo} is eventually obtained using (1). As a result, the HiLo technique provides a powerful method for fast two-dimensional image acquisition, since the measurement rate equals half of the camera framerate.

3. Experimental setup

In Fig. 1 the experimental setup of the HiLo microscope with an adaptive lens is illustrated. The illumination is created using a 532 nm laser diode, coupled into a multi mode fiber. The multi mode fiber is fixed onto a magnetic metal sheet and can be vibrated by an alternating magnetic field. Consequently, a nonuniform, speckle-patterned as well as a uniform illumination can be realized with a static and vibrating fiber, respectively. The so generated nonuniform or uniform illumination is collimated by the lenses L1 and L2. After passing the beam splitter (BS), the light enters the illumination arm of the microscope. Here, the light is focused to the sample by a lens system consisting of the adaptive lens (AL) with NA ≈ 0.05 and refractive power $1/f_{\mathrm{AL}} = -24 \ldots 25\,\mathrm{m}^{-1}$ (see Fig. 2) and the objective lens (OL) with NA $= 0.55$ and $f_{\mathrm{L}} = 4.5$ mm. The objective lens is required for achieving a sufficient axial resolution, since the NA of the adaptive lens is too low. The distance between the two lenses amounts to 26 mm. Another lens (L3) with $f_3 = 40$ mm is then used to image the light onto a CCD camera (pco pixelfly, dynamic range 14 Bit and pixel size 6.45 µm). A long-pass filter with the cut-on wavelength 550 nm (Thorlabs

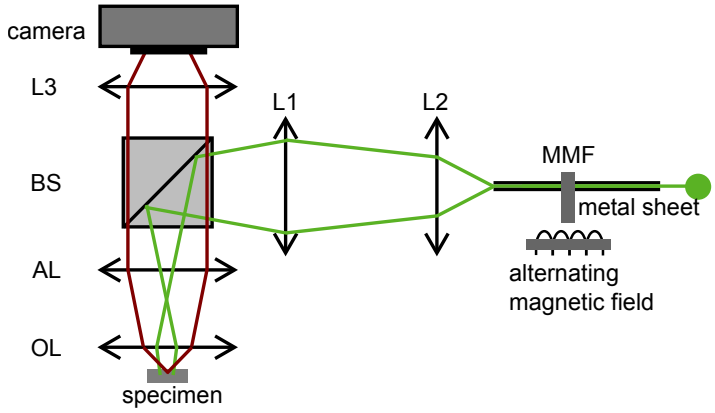

Fig. 1. Experimental setup. A laser beam is coupled into a multi mode fiber (MMF) that can be vibrated by alternating magnetic fields. After passing a beam splitter (BS), the light is focused into the sample by a combination of an adaptive (AL) and an objective lens (OL). The fluorescence light passes the same optical path backwards and is eventually detected by a camera.

FEL0550) is placed directly in front of the camera for fluorescence measurements.

The adaptive lens used for axial scanning is based on the principle described in [23]. The adaptive lens consists of a transparent Polydimethylsiloxane (PDMS) membrane into which an annular piezo bending actuator is embedded. An incompressable transparent fluid is filled between the membrane and the glass substrate. When actuated, the piezo generates a pressure in the lens which deflects the membrane and thus changes the refractive power. This technique enables a large tuning range of the refractive power between $1/f = -24 \ldots 25\,\mathrm{m}^{-1}$ with applied voltages between -40 V and 40 V, see Fig. 2(a). The resonance spectrum of the membrane cen-

#265224 Received 16 May 2016; accepted 20 Jun 2016; published 23 Jun 2016

ter point deflection in Fig. 2(b) shows that the first resonance mode appears at 250 Hz and hence driving up to this frequency is possible, although the refractive-power vs. voltage characteristics is different at resonance mode.

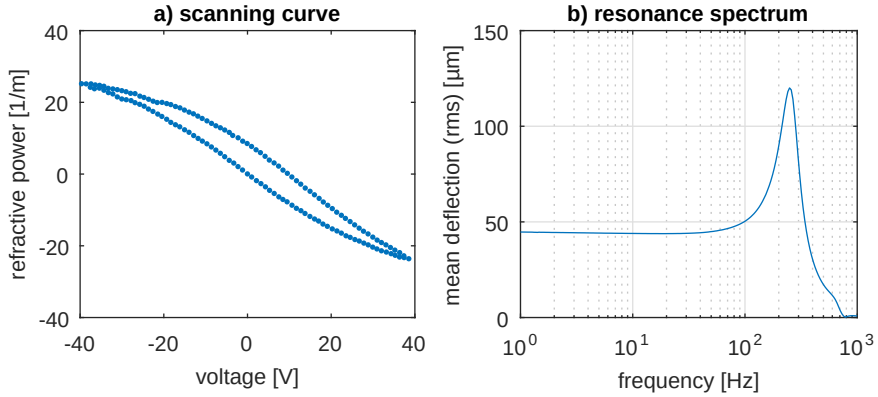

Fig. 2. a) Refractive power of the adaptive lens as a function of the applied voltage with hysteresis behaviour. b) resonance spectrum of a similar electrically tunable lens.

4. Characterization

The relevant properties of the AL-HiLo are discussed in this section. In order to determine these properties, a home-built specimen is used. Several rhodamine B-marked micro particles based on melamine resin are placed onto a glass platelet. The diameter of the micro particles amounts to 10 µm with a standard deviation below 0.3 µm according to the manufacturer. Since the HiLo algorithm is based on the evaluation of the speckle-patterns of the non-uniform illumination, in Section 4.1 an overview of the illumination is given.

4.1. Illumination

A small speckle size is desirable, because in HiLo microscopy the axial resolution is inversely proportional to the speckle frequency and thus scales with speckle size. Additionally, a higher amount of speckles in the evaluation area means higher stability in the speckle contrast determination and thus better lateral imaging quality. However, if the smallest speckles size is smaller than 2 px, the speckle contrast is reduced (a speckle size of 1 px leads to a reduction of the speckle contrast by 30 %) [24]. To address these competing requirements, we aimed for a minimal speckle size in the range of $1.5-2$ px on the camera, when the sample is in-focus. We employ a multi mode fiber for the generation of the nonuniform illumination, because it produces fully developed speckles and also provides a high transmission of the laser light. The characteristics of the resulting speckle illumination can be tuned by the numerical aperture NA and the diameter a of the fiber. The minimal speckle size Δs of the multi mode fiber used in our setup amounts to $\Delta s = \frac{\lambda}{2\cdot \mathrm{NA}} = 103$ nm and the speckle number is $N = \pi(a/\Delta s)^2 = 3\cdot 10^8$ [25]. The measured speckle size on the camera of in-focus images is between 1.5 px and 1.6 px over the whole applied actuation voltage range. Taking into account the magnification of the microscope (cf. section 4.3), the speckle size on the in-focus plane of the specimen varies between 360 nm and 690 nm depending on the actuation voltage of the tunable lens. Since no correlation between the speckle size on the camera and the actuation voltage of the tunable lens is observable, the size A of the evaluation window for the contrast determination in the HiLo algorithm is held constant for all actuation voltages ($A = 7$ px).

#265224 Received 16 May 2016; accepted 20 Jun 2016; published 23 Jun 2016

4.2. *Axial scanning*

In this section the axial displacement of the focus plane is determined as a function of the actuation voltage of the tunable lens. For this purpose the home-built specimen with the fluorescent beads is used as specimen and an axial scan using a motorized stage is conducted for each actuation voltage. In order to obtain the focus position, the integrated intensity of the resulting HiLo images is determined in dependency of the axial position. As depicted in Fig. 3, a total scanning range of 1 mm is covered. Note that the tuning range can be adjusted by varying the distance between adaptive and objective lens. The axial displacement function is nonlinear and shows hysteresis behavior (as expected due to the characteristics of the tunable lens, cf. Fig. 2). As will be shown in the following sections, HiLo microscopy is a suitable tool to cope with

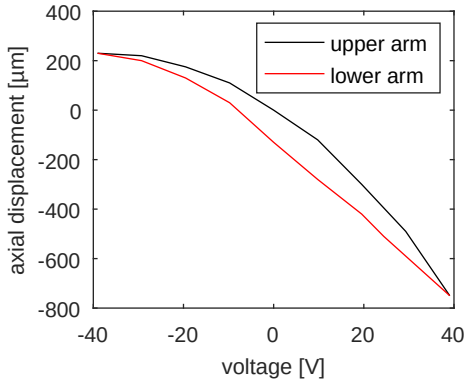

Fig. 3. Axial scanning curve: Axial displacement as a function of the actuation voltage of the electrically tunable lens.

these challenges. In the interests of clarity, the characterizations in the following sections are only shown for the lower path of the axial scanning curve (cf. red curve in Fig. 3).

4.3. *Lateral magnification*

The lateral magnification of the AL-HiLo at 0 V actuation voltage of the electrically tunable lens is determined using a 1951 USAF resolution test chart (Thorlabs R1DS1P). Here, the lateral magnification amounts to 20.2. Given a camera resolution of 1392×1040 pixels, a total lateral area of $447 \times 335\,\mu\text{m}^2$ can be observed on the specimen. Note that the observable area as well as the magnification of the system can be adapted to requirements of a given application by changing lens L3 and/or changing the distance to the camera.

As the refractive power decreases with increasing actuation voltage (cf. Fig. 2(a)), the lateral magnification is expected to decrease with increased actuation voltage. In order to characterize the relative change of the magnification, the home-built specimen consisting of fluorescent beads on a glass plate is used. For every actuation voltage, the specimen is moved into the focus (cf. Fig 4a). The relative magnification m_r is determined as the quotient $m_\text{r}(U) = d_p(U)/d_p(0\,\text{V})$, with d_p being the distance between two characteristic beads. The resulting relative magnification as a function of the actuation voltage U is illustrated in Fig. 4(b). The absolute magnification varies between 27.3 and 13.7. The observable area ranges between $334 \times 250\,\mu\text{m}^2$ at -40 V and $660 \times 495\,\mu\text{m}^2$ at 40 V actuation voltage of the lens. Since the speckle size does not scale with the actuation voltage, the parameters of the HiLo algorithm do not have to be adjusted for each axial position. Consequently, the final HiLo images only have to be re-scaled in order to compensate the voltage-dependent magnification.

#265224 Received 16 May 2016; accepted 20 Jun 2016; published 23 Jun 2016

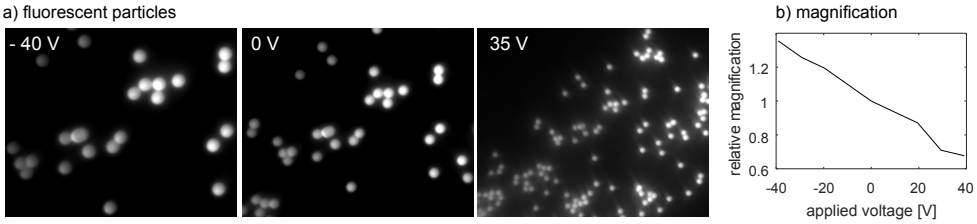

Fig. 4. Images of a) fluorescent particles with varying voltage applied at the adaptive lens. The images of the fluorescent particles are a 491x400 pixels-sized subimage taken out of the middle of the original camera images. b) The resulting relative magnification normalized to the magnification with 0 V actuation voltage.

4.4. Spatial resolution

The upper threshold of the AL-HiLo lateral resolution amounts to

$$\mathrm{FWHM}_{x,y} = \frac{0.37\lambda}{\mathrm{NA}_{\mathrm{eff}}(U)} \leq 500\,\mathrm{nm} \tag{7}$$

with the effective numerical aperture $\mathrm{NA}_{\mathrm{eff}}(U)$ of the lens system consisting of AL and OL with $0.34 \leq \mathrm{NA}_{\mathrm{eff}}(U) \leq 0.55$ for the full actuation voltage U range. Element 6 of group 7 of the 1951 USAF resolution test chart (Thorlabs R1DS1P) is resolved clearly for all voltages applied at the electrically tunable lens. Consequently, both the theoretical and experimental lateral resolution should be well below 2 µm.

The axial resolution of the microscope is determined theoretically using the full-width-half-maximum (FWHM) of the point spread function. According Ford et al. [14], the three-dimensional point spread function can be calculated analytically by assuming similar excitation and detection wavelength and applying the Stokseth [26] approximation. As a result, the axial resolution of the low-frequency component equals

$$\mathrm{FWHM}_{\mathrm{Lo}} \approx \frac{0.54}{\kappa_{\mathrm{S}} \cdot \mathrm{NA}_{\mathrm{eff}}(U)} \tag{8}$$

with the speckle frequency $\kappa_{\mathrm{S}} \approx m_{\mathrm{r}}/(2\Delta_{\mathrm{S}})$, whereby Δ_{S} denotes the speckle size on the camera and m_{r} the lateral magnification (cf. Fig. 4). The effective numerical aperture NA is numerically determined for the lens system consisting of the adaptive lens (AL) and the objective lens (OL) using the tuning curve of Fig. 2. The FWHM of the high-frequency component is

$$\mathrm{FWHM}_{\mathrm{Hi}} \approx \frac{0.68}{\kappa_{\mathrm{c}} \cdot \mathrm{NA}_{\mathrm{eff}}(U)} \tag{9}$$

with the cutoff frequency κ_{c} (cf. Section 2). As shown in Fig. 5(a), the resulting calculated axial resolution for the Hi- and Lo-components is between 3.3 µm and 5.4 µm and between 900 nm and 2.3 µm, respectively, depending on the actuation voltage of the adaptive lens. The decreased effective NA with increased absolute value of the actuation voltage of the adaptive lens leads to a deterioration of the axial resolution with increased actuation voltage. While the resulting axial resolution of the Hi-component is best at 0 V actuation voltage, the axial resolution of the Lo-component enhances with negative actuation voltage of the adaptive lens, because of the increasing magnification m_{r} and thus increasing speckle frequency κ_{S}.

The axial resolution is determined experimentally by using the images obtained in section 4.2, where an axial scan using a motorized stage was conducted for each actuation voltage.

#265224 Received 16 May 2016; accepted 20 Jun 2016; published 23 Jun 2016

The FWHM of the corresponding optical sectioning curves determines the axial resolution of the AL-HiLo. Assuming Gaussian shaped intensity profiles of the beads as well as a Gaussian shaped point spread function of the microscope, the resulting axial resolution $\mathrm{FWHM}_{\mathrm{HiLo,exp}}$ is obtained by

$$\mathrm{FWHM}_{\mathrm{HiLo,exp}} = \sqrt{\mathrm{FWHM}^2_{\mathrm{measured}} - d^2_{\mathrm{bead}}} \tag{10}$$

with measured $\mathrm{FWHM}_{\mathrm{measured}}$ of the optical sectioning curve and bead diameter $d_{\mathrm{bead}} = 10\,\mu\mathrm{m}$ according to the manufacturer. The errorbars in Fig. 5 indicate the standard deviation of the axial resolution that is calculated by error propagation of the standard deviation of the particle size. The experimentally and theoretically obtained axial resolutions are generally in good agreement, whereby the experimentally obtained axial resolutions for the Lo-component seem to face a alight, almost constant shift compared to the theoretical data. This might on the one hand be an effect of the small speckle size of 1.6 px on the camera and consequently a reduced effective speckle contrast [24]. On the other hand, the speckles in the out-of-focus images might be only partially developed, making them sensitive to some aberrations [27]. However, the overall good fit between experimental and theoretical data suggest, that these effects are small and can be neglected in most scenarios. As a result, aberrations do not negatively affect the axial resolution within uncertainty limits.

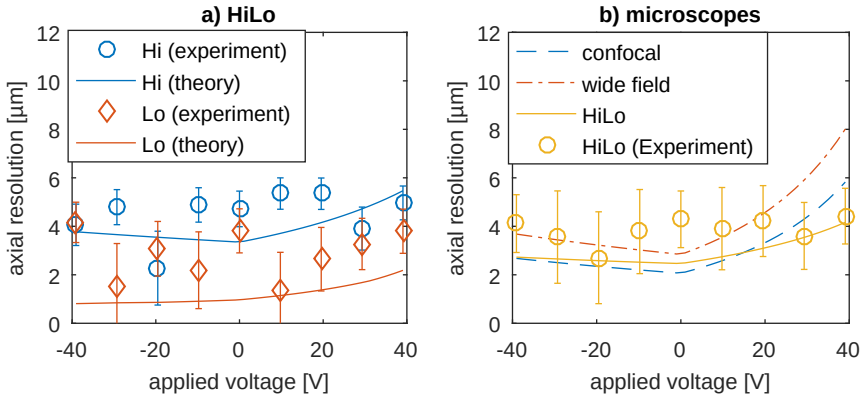

Fig. 5. a) Experimentally and theoretically obtained axial resolution (FWHMs of the point spread function) for high- and low-frequency components of HiLo images. b) Axial resolution of overall HiLo microscopy as well as for confocal and widefield microscopy with identical objectives.

In order to evaluate the HiLo microscope against state-of-the-art techniques, the axial resolution of classical confocal and widefield microscopy are calculated according to [28]

$$\mathrm{FWHM}_{\mathrm{WideField}} = \frac{0.88\lambda}{n - \sqrt{n^2 - \mathrm{NA}^2}}, \quad \mathrm{FWHM}_{\mathrm{Confocal}} = \frac{0.64\lambda}{n - \sqrt{n^2 - \mathrm{NA}^2}}. \tag{11}$$

Compared to confocal microscopy, HiLo provides similar axial resolution for actuation voltages of the adaptive lens between -40 V to 20 V and even an enhanced resolution for voltages above 20 V, as shown in Fig. 5(b). In conclusion, the axial resolution is about 4 µm over the full scanning range.

4.5. Depth of field adjustment

One of the main benefits of the HiLo technique is the possibility to adjust the depth of field (DOF) a-posteriori by choosing an appropriate depth-of-field multiplier σ_w^{-1} [12]. This

#265224 Received 16 May 2016; accepted 20 Jun 2016; published 23 Jun 2016

enables flexible scans that compensate the unevenly distributed measurement positions caused by the nonlinear relation between axial displacement and actuation voltage of the electrically tunable lens (cf. Fig. 3(a)). This principle is demonstrated in Fig. 6 using optical sectioning curves at varying actuation voltages. Analogously as in Section. 4.2 an axial scan is performed over the home-built specimen for each actuation voltage using a motorized stage. The optical sectioning curves are then determined by integrating the intensity of the obtained HiLo images. As can be seen in Fig. 6, the distance between the peak positions increases with increasing voltages. Consequently, the depth-of-field (DOF) is also increased with this actuation voltage by tuning the depth-of-field parameter σ_w in order to compensate for this unevenly distributed axial measurement positions. As a consequence, the optical sectioning curves intersect at half of the maximum normalized intensity. That implies a complete covering of the scanned axial position with optimal use of the obtained frames.

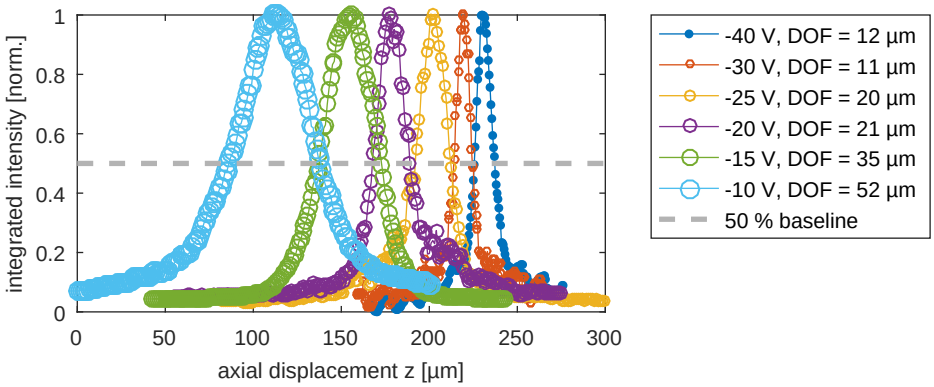

Fig. 6. a) Optical sectioning curves of HiLo images for six selected actuation voltages. Adjusting the depth-of-fields (DOF) of the HiLo mechanism ensures that the full axial range is covered. Simultaneously the optical sections are as thin as possible.

In conclusion, the HiLo technique is able to compensate the main drawbacks of axial scanning using an electrically tunable lens, namely deteriorating axial resolution caused by aberrations and unevenly distributed axial measurement positions caused by the nonlinear axial displacement function (cf. Fig. 3). Furthermore, volumetric HiLo microscopy profits from the main advantages of axial scanning. On the one hand HiLo is able to exhaust the potential for high speed measurements, because HiLo provides a full frame by only acquiring two images and thus is in principle capable for measurement times of the half of the camera exposure and acquisition time. On the other hand, adaptive HiLo microscopy does not rely on any mechanical scanning, because axial scanning is conducted using the electrically tunable lens and lateral scanning is not required because of the wide field of view enabled by the HiLo technique.

5. Measurements

In this section volumetric measurements are conducted by tuning the actuation voltage of the lens. A compensation for the voltage-dependent magnification is conducted by re-scaling the images after the HiLo algorithm is executed. Since the speckle size does not change with varying voltage, no adaption of the HiLo technique is necessary.

Two different operation modi of the axial scan using the tunable lens are possible:

(a) one scanning cycle with uniform- and a second cycle with nonuniform-illumination

#265224 Received 16 May 2016; accepted 20 Jun 2016; published 23 Jun 2016

(b) alternating images with uniform and nonuniform illumination directly after each other.

Modus (a) has the advantage, that the scanning process is faster than for modus (b), because there is less time needed for switching the illumination source. In contrast, modus (b) is more robust against the hysteresis behavior of the electrically tunable lens as well as cross-sensitivities between refractive power of the lens and ambient atmospheric pressure and temperature. Since at this stage speed is not in the scope of this paper, we use the second modus in our setup.

The following measurements are conducted with a actuation voltage step width of 40 mV.

5.1. Demonstration measurement

In order to demonstrate the optical sectioning and axial scanning capability of the adaptive HiLo microscope, a specimen consisting of several fluorescent beads with a diameter of about 10 µm separated by a thin foil is investigated. In Fig. 7(a-c) the uniformly illuminated images are shown for different axial scanning depths, whereby HiLo images for different scanning depths are shown in 7(d-f). While the marked beads are visible in all images obtained by using the uniform illumination, the out-of-focus contributions are rejected in the HiLo images.

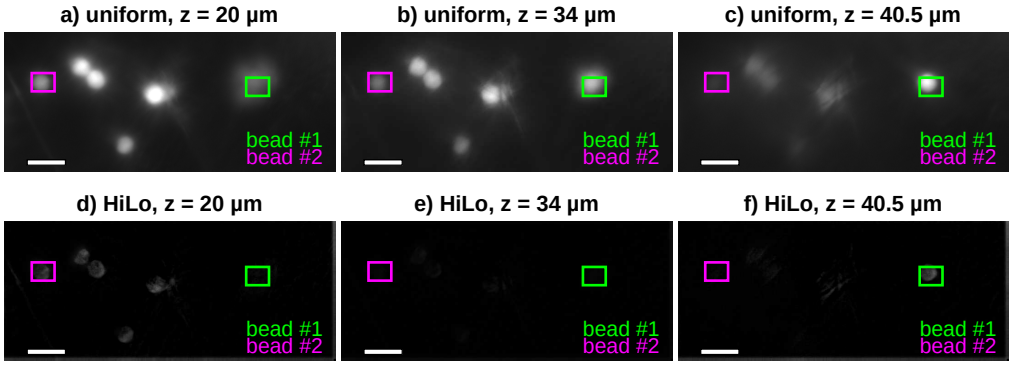

Fig. 7. a-c) Selected images with uniform illumination. d-f) Selected HiLo images for different axial planes. The axial scanning is conducted by tuning the adaptive lens.

For a clearer illustration of the optical sectioning capability, the integrated intensity in the marked region-of-interests is integrated along z-direction. As depicted in Fig. 8, the HiLo algorithm enables optical sectioning in contrast to the standard widefield technique.

5.2. Zebrafish measurements

The microscope is used for investigating reporter gene-driven fluorescence in the thyroid gland of zebrafish embryos. Zebrafish embryos are used as experimental model in basic and applied research since the large number of produced embryos, their size and optical transparency provide various experimental advantages and screening opportunities. Furthermore, the principal similarity of vertebrates allow to derive information relevant for understanding of human diseases. Particularly their high transmission rate makes them an ideal candidate for optical measurements. Transgenic zebrafish embryos have been used to understand the dynamics of thyroid morphogenesis [29]. Here, the thyroid is marked with the mCherry protein[30]. The maximum excitation wavelength is 587 nm. With a quantum yield of 0.22, this amounts to a fluorescence yield of 8.36 % at the used laser wavelength of 532 nm. The maximum emission wavelength is 610 nm. The resulting fluorescence HiLo images of a thyroid gland follicle are

#265224 Received 16 May 2016; accepted 20 Jun 2016; published 23 Jun 2016

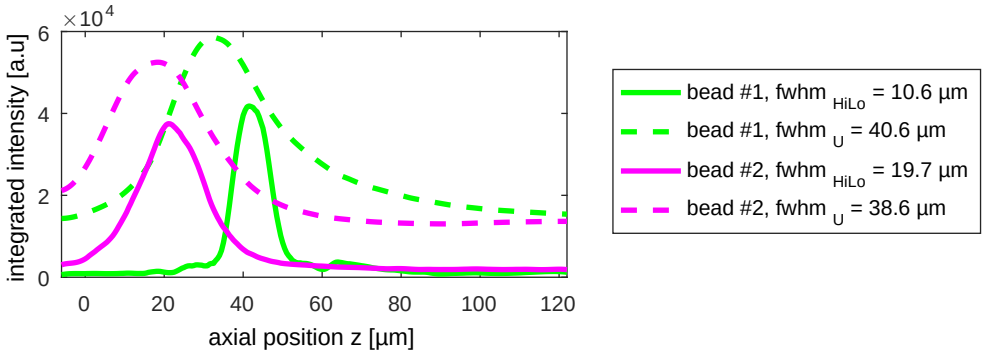

Fig. 8. Dotted lines: integrated intensity for selected beads (cf. Fig. 7) along axial direction in uniform illumination images. Solid lines: integrated intensity for HiLo images.

depicted in Fig. 9. For the sake of clarity, only selected frames between $-13.8\,\mathrm{V}$ and $-21.6\,\mathrm{V}$ actuation voltage with an region-of-interest of size 271×351 pixels are shown. The HiLo images have increased contrast due to the rejection of background signals. As a result, the structure of one gland follicle of the thyroid becomes visible in contrast to the measurements with uniform illumination.

6. Conclusion and outlook

The presented volumetric HiLo microscope with an adaptive lens for axial scanning provides a scanning range of about 1 mm with an axial resolution of about 4 µm and sub-micron lateral resolution. In contrast to confocal microscopy with electrically tunable lenses [16], the axial resolution of the HiLo microscope is not significantly reduced by aberrations of the optical components. Consequently, HiLo microscopy is a promising tool to be combined with the advantages of adaptive lenses for axial scanning. Furthermore, the a-posteriori adjustment of the depth-of-field is used to create flexible scans that compensate for the nonlinear relation between actuation voltage of the lens and the axial displacement. As a result, the AL-HiLo enables reliable measurements along the full depths of the specimen.

The HiLo microscope employing an adaptive lens is not without its limitations. In the current setup, the magnification as well as the observable area strongly scales with the actuation voltage of the lens, varying between 27 and 14. Although the voltage-dependent magnification can be corrected after the measurement, the observable area is limited for low applied voltages, going down to 334×250 µm. The application of another electrically tunable lens in the detection arm (after lens L3) could be used for proper imaging to the camera and thus a constant lateral magnification.

For this proof-of-principle microscope, the measurement rate for the HiLo images is about 2 Hz. The acquisition time is mainly limited by the decay time of the fiber vibration for the generation of the uniform illumination and non-optimized synchronization of the adaptive lens and the alternating magnetic field that generates the uniform illumination. However, first investigations suggest, that the acquisition time for one HiLo image can be reduced to about $T_{\mathrm{HiLo}} \approx 2T_{\mathrm{Exposure}}$, assuming exposure times $T_{\mathrm{Exposure}} \geq 60\,\mathrm{ms}$. While shorter exposure times would allow faster scans, biological samples e.g. zebrafish embryos are prone to the consequently required higher laser intensities because of photobleaching and phototoxicity. The type of adaptive lens that is used in our adaptive HiLo microscopy provides tuning frequencies up to about 200 Hz and is thus not a speed limiting factor. As a consequence, the exposure time (restricted by the sensitivity of the specimen) is the dominant contribution to the overall

#265224 Received 16 May 2016; accepted 20 Jun 2016; published 23 Jun 2016

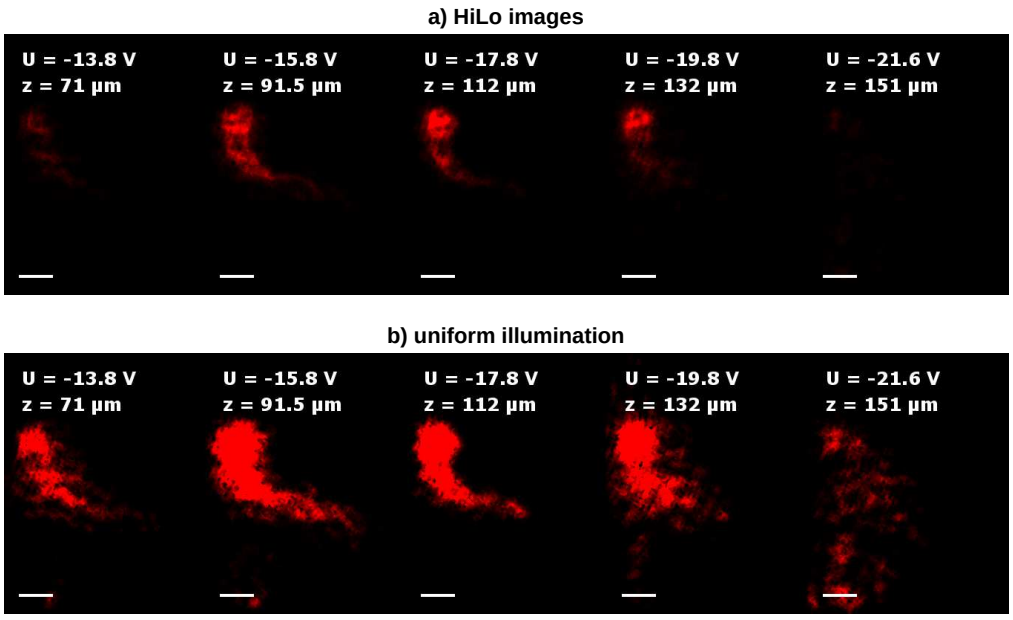

Fig. 9. a) HiLo images and b) images with uniform illumination of reporter-gene driven mcherry fluorescence of transgenic zebrafish. The fluorescence is regulated by part of the promotor region of the thyreoglobulin gene, coding for a thyroid hormone precursor. The optical sectioning provided by the HiLo algorithm leads to the rejection of the out-of-focus contributions and thus increased contrast of the images compared to the uniformly illuminated images. Scalebar is 10 µm.

measurement time of the full specimen. As a result, the prospective time for a full volumetric characterization should be approximately $2NT_{\text{Exposure}}$ with N being the number of frames per axial scan.

As a demonstration of the optical sectioning capability of the AL-HiLo microscope, a home-built specimen and a transgenic zebrafish embryo was investigated. In contrast to wide field microscopy, the contrast of the HiLo images was increased due to the rejection of out-of-focus signals. The huge field-of-view of the HiLo microscope and the high axial scanning range of the tunable lens enables three-dimensional measurements over a huge volume. The potentially high scanning frequency of the tunable lens up to 250 Hz and no need for lateral scanning makes the AL-HiLo a promising candidate for high-throughput characterization of zebrafish embryos such as functional genetics to study organ differentiation or responses to drug/chemical exposure.

Acknowledgments

The financial support of the Deutsche Forschungsgemeinschaft (DFG) for the project CZ 55/32-1 and Wa1657-6 is gratefully acknowledged. The authors also thank Hannes Radner for providing the controlling of the adaptive lens. We thank Stefan Scholz of Helmholtz Centre for Environmental Research GmbH for providing the samples and fruitful discussions.